High Power Laser Science and Engineering, (2024), Vol. 12, e40, 12 pages.
doi:10.1017/hpl.2024.20

HIGH POWER LASER SCIENCE AND ENGINEERING

RESEARCH ARTICLE

A 301 W narrow-linewidth in-band pumped Er:Yb co-doped fiber amplifier at 1585 nm and related modeling for dynamics study and optimization

Guohao Fu[1,2], Guanzhong Li[1,2], Weilong Yu[1,2], Pei Li[1,2], Dan Li[1,2], Qirong Xiao[1,2], Mali Gong[1,2], and Ping Yan[1,2]

[1] *Department of Precision Instrument, Tsinghua University, Beijing, China*

[2] *State Key Laboratory of Precision Space-time Information Sensing Technology, Beijing, China*

(Received 9 December 2023; revised 26 February 2024; accepted 25 March 2024)

Abstract

To overcome Yb lasing, a kilowatt-level 1535 nm fiber laser is utilized to in-band pump an Er:Yb co-doped fiber (EYDF) amplifier. The output power of a 301 W narrow-linewidth EYDF amplifier operating at 1585 nm, with 3 dB bandwidth of 150 pm and $M^2 < 1.4$, is experimentally demonstrated. To the best of our knowledge, it is the highest output power achieved in L-band narrow-linewidth fiber amplifiers with good beam quality. Theoretically, a new ion transition behavior among energy levels for in-band pumping EYDF is uncovered, and a spatial-mode-resolved nonlinearity-assisted theoretical model is developed to understand its internal dynamics. Numerical simulations reveal that the reduction in slope efficiency is significantly related to excited-state absorption (ESA). ESA has a nonlinear hindering effect on power scaling. It can drastically lower the pump absorption and slope efficiency with increasing pump power for in-band pumped EYDF amplifiers. Meanwhile, optimized approaches are proposed to improve its power to the kilowatt level via in-band pumping.

Keywords: Er:Yb co-doped fiber amplifier; excited-state absorption; in-band pumping; ion transition behavior; spatial-mode-resolved nonlinearity-assisted theoretical model

1. Introduction

High-power fiber lasers operating in the 1.5 μm band have attracted great interest for a wide range of scientific research and applications, for example, free space optical communication[1,2], third-generation gravitational wave detection[3,4] and eye-safe LIDAR[5], and are used as the in-band pump source for high-power Tm-doped fiber lasers[6]. Over the past decades, high stability, compactness and perfect heat dissipation have been achieved by utilizing all-fiber master oscillator power amplifiers in amplifying the 1.5 μm band laser. The challenge of the small absorption cross-section and ion pair-induced quenching (PIQ) in Er-doped fiber (EDF) has been overcome by co-doping with Yb ions that can absorb pump lasers with the wavelength of 9xx/10xx nm and transfer the energy to Er ions by cross-relaxation[7]. However, while a 20-kW single-mode fiber laser at the 1 μm band[8] and 1-kW fiber amplifiers emitting at the 2 μm band[9] have already been achieved, the power of 1.5 μm fiber amplifiers has stagnated at a few hundred watts.

In 2007, a 297 W fiber laser operating at 1567 nm, using a homemade 30/600 μm Er:Yb co-doped fiber (EYDF) pumped by 975 nm laser diodes (LDs), was reported, and the slope efficiency decreased from 40% to 19% at high output power due to the Yb parasitic laser stemming from Yb amplified spontaneous emission (ASE)[10]. To raise the threshold of the Yb parasitic laser, off-peak pumping has been proposed in recent years, for example, by using pumping wavelengths that deviate from the absorption peak at 975 nm, such as 915, 940 and 1018 nm[11–14]. In 2020, by 915 nm pumping, a single-mode 1560 nm 25/300 μm EYDF amplifier with an output power of 302 W was demonstrated, the highest single-mode power from EYDF to date[11]. In 2021, using 1018 nm pumping, our group demonstrated an EYDF amplifier operating at 1600 nm with a record power of 220 W[14]. In 2023, by adopting 940 nm pumping and inserting a Yb-doped fiber in front of the amplifier to inhibit Yb-ASE, an EYDF amplifier with an output power of 345 W at 1535 nm was reported, which is so far the highest power

Correspondence to: P. Yan, Department of Precision Instrument, Tsinghua University, Beijing 100084, China. Email: pyan@mail.tsinghua.edu.cn

achieved in all-fiber EYDF amplifiers[13]. The Yb parasitic laser prevented a further increase in power. Therefore, although Yb-ASE can be suppressed by off-peak pumping, Yb-ASE is still a critical limitation for further power scaling of EYDF amplifiers. To avoid Yb-ASE in EYDF amplifiers completely, researchers have invented 1480/1535 nm in-band pumping[15–18]. Because there is no Yb-ASE and a low quantum defect, EYDF amplifiers utilizing in-band pumping are expected to achieve a much higher power than any other pumping methods. However, the output power of in-band pumped EYDF amplifiers is still lower than that of other pumping schemes currently, due to the low pump power and brightness of the 1535 nm pumping laser[15,16]. Theoretically, although some theoretical studies of energy transfer for EYDF pumped by a 9xx/10xx nm laser have been reported[19–21], the modeling and dynamic study of in-band pumped EYDF amplifiers have been rarely reported, and are desirable to help us understand its underlying mechanisms.

In this paper, we numerically and experimentally verify the underlying capability of in-band pumped EYDF amplifiers in enabling higher output power. Based on kilowatt-level 1535 nm in-band pumping, a 1585 nm, 301 W, narrow-linewidth EYDF amplifier with good beam quality is demonstrated. We employ a ring-cavity narrow-linewidth laser operating at 1585 nm as a seed source, which has a narrower linewidth compared to previously reported oscillators that use fiber Bragg gratings[10,11]. The 3 dB bandwidth is about 150 pm at the highest power. The kilowatt-level 1535 nm laser is gained by the combination of many 1535 nm fiber lasers. The 1535 nm fiber laser was reported earlier by our group[22]. To the best of our knowledge, it is the highest output power achieved in L-band narrow-linewidth fiber amplifiers with a good beam quality of $M^2 < 1.4$. Further increasing power leads to heat damage of the fusion-splicing point. Meanwhile, based on our proposed ion transition behavior among energy levels regarding in-band pumping, a spatial-mode-resolved nonlinearity-assisted theoretical model accounting for excited-state absorption (ESA) and PIQ is built to uncover the dynamic process in EYDF amplifiers. Owing to temporal fluctuation induced by the beat frequency of longitudinal modes and other intensity noise that may derive from the interaction of both PIQ and modulation instability in anomalous dispersion, it is necessary to consider nonlinearity in the model. Hence, the simulation results of the output power, spectral broadening, evolution of beam quality, slope efficiency and pumping absorption are in great agreement with the experimental results.

Numerical simulation demonstrates that the decrease in laser efficiency is significantly associated with PIQ and ESA. The distinction is that the influence of PIQ on output power is linear, while that of ESA is nonlinear. ESA is the main factor prompting pump absorption and slope efficiency to decrease with increasing pump power. This work can deepen our understanding of the dynamics for in-band pumped EYDF amplifiers with a more complex ion transition process. The simulation predicts that a kilowatt-class EYDF amplifier operating in the L band could be possible by suppressing ESA and PIQ, increasing the Er ion concentration, optimizing the fiber length, increasing the core-to-cladding ratio and optimizing the central wavelength.

2. Experimental setup

A schematic of the established high-power EYDF laser system is illustrated in Figure 1. The experimental setup was an all-fiber structure composed of three parts: a seed source, two-stage pre-amplifiers and a main amplifier. The seed source was a ring cavity and could be tuned in the L band via a Fabry–Pérot filter (FPF). The FPF had a very narrow bandwidth, enabling narrow-bandwidth laser output from

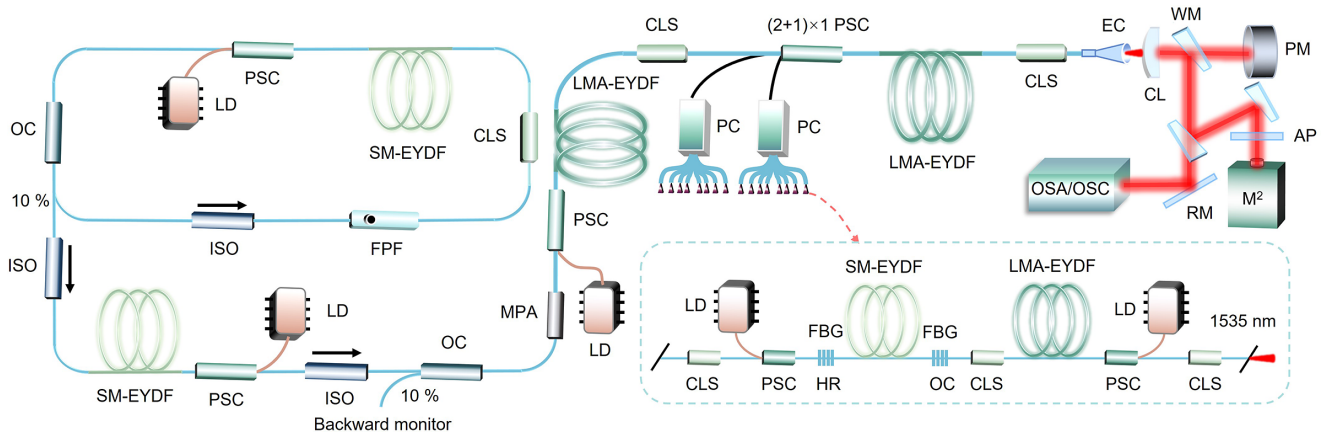

Figure 1. Configuration of the high-power Er-Yb co-doped fiber laser system. SM-EYDF and LMA-EYDF represent 10/125 μm and 25/300 μm EYDF, respectively. CL, collimating lens; WM, wedge mirror; PM, power meter; RM, reflective mirror; AP, attenuation plate; HR-FBG, high-reflectivity fiber Bragg grating; OC-FBG, output coupler fiber Bragg grating; LD, laser diode; PSC, pump signal combiner; CLS, cladding light stripper; FPF, Fabry–Pérot filter; ISO, isolator; MFA, mode field adapter; PC, pump combiner.

https://doi.org/10.1017/hpl.2024.20 Published online by Cambridge University Press

the seed cavity. In the cavity, 5 m long 10/125 μm EYDF with a 3.5 dB/m absorption at 915 nm was forward pumped by a 915 nm LD, and an output coupler (OC) extracted 10% power from the cavity. The output power of the laser from the cavity was about 80 mW, with a bandwidth of 70 pm. In sequence, the seed was pre-amplified by two types of EYDF pumped by a 915 nm LD. A 5 m long 10/125 μm EYDF was applied as the first stage pre-amplifier; then, an OC was spiced to monitor backward light. A mode field adapter (MFA) was used to guarantee beam quality and coupling efficiency. The power after the first pre-amplifier was about 2 W. Then, 7 m long 25/300 μm EYDF was exploited as the second pre-amplifier. A cladding light stripper (CLS) was used to strip high-order modes (HOMs) and the residual pump that would affect the subsequent main amplifier. The main amplifier was built by 50 m long homemade 25/300 μm EYDF (numerical aperture (NA) = 0.09, core absorption = 72 dB/m@1535 nm) in-band pumped by 16 fiber laser modules emitting at 1535 nm. These modules were combined by using a (2 + 1) × 1 pump signal combiner and two pump combiners (PCs). Each 1535 nm module could provide nearly 150 W pump power. So, the total power of the 1535 nm pump source could reach 2400 W. An illustration of the 1535 nm module is presented inside the dotted box in Figure 1, introduced in Ref. [22]. Notably, the gain fiber length of the main amplifier was much longer than the calculated results based on the absorption coefficient given by its test report, which is because the ESA could considerably reduce the absorption coefficient in the experiment, which will be discussed later. Finally, a CLS eliminated the residual pump and HOMs. An end cap (EC) was used to protect the output fiber end. In the measuring part, a plano-convex lens was used to collimate the output laser. Then, the laser was measured by a power meter, an M^2 measurement system (Thorlabs BP209-IR2/M) and other measuring devices.

3. Experimental results and discussion

It should be mentioned that there is no self-absorption in 50 m EYDF at the main amplifier, according to our experimental test. Long gain fiber can efficiently redshift the gain spectrum to the L band, but which laser wavelength is the most appropriate is worth finding out. Our experiment compares the laser properties at different wavelengths in the L band. To get higher power and retain weak ASE in the 1.5 μm band, 1585 nm is the most suitable wavelength. The measured output power and corresponding slope efficiency versus pump power are shown in Figures 2(a) and 2(b). A maximum power of 301 W is obtained, but the slope efficiency is low and it gradually decreases as pump power increases (Figure 2(b)). The spectrum at a large wavelength span versus signal power is illustrated in Figure 2(c). As output power increases, the ASE component on the spectrum is gradually amplified. The approximately 1545 nm ASE comes from the first pre-amplifier because of the highest gain at the C band induced by its short gain fiber. Then, it is amplified in sequent EYDF. The near 1607 nm ASE is from the main amplifier due to gain redshift induced

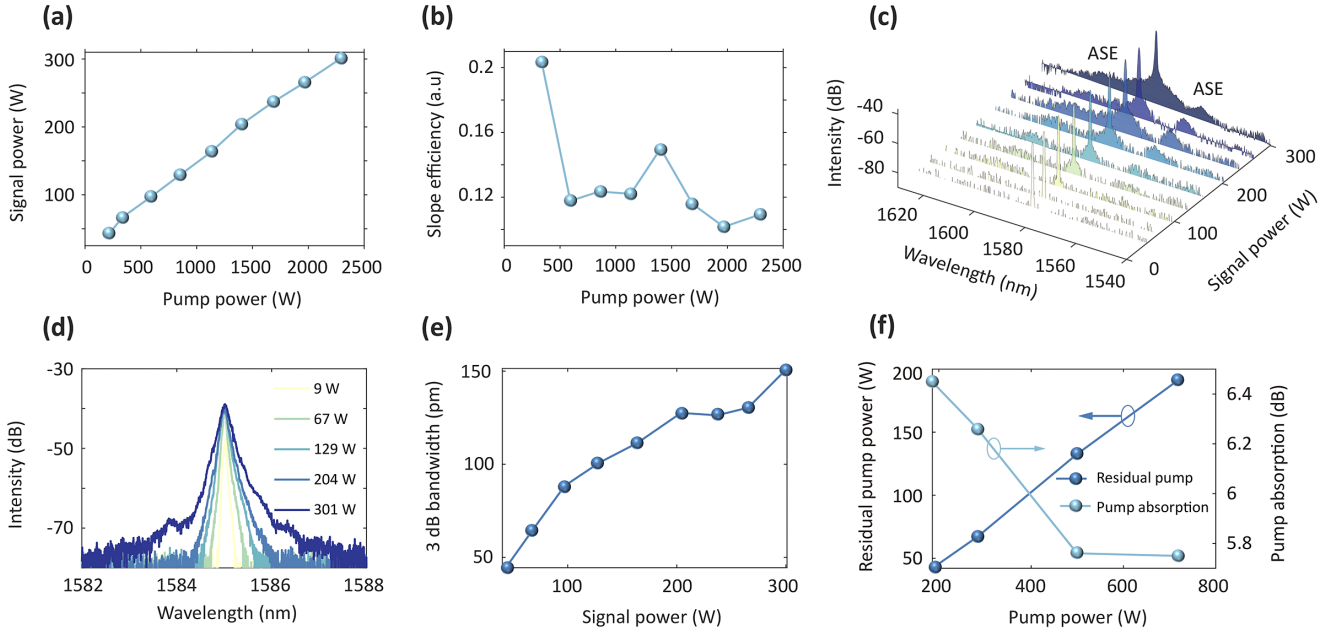

Figure 2. Experimental results of the in-band pumped EYDF amplifier. (a) Signal power versus pump power. (b) Corresponding slope efficiency. The slope efficiency $\eta\left(P_{\mathrm{p}}\right)$ is defined as $\Delta P_{\mathrm{s}}/\Delta P_{\mathrm{p}}$, the proportion of the power that will transfer from the injected pump to the signal laser. (c) Spectrum changes with pump power at a large wavelength span. (d) Spectral evolution at a small wavelength span. (e) 3 dB bandwidth of laser versus signal power. (f) Residual pump power and pump absorption versus pump power.

https://doi.org/10.1017/hpl.2024.20 Published online by Cambridge University Press

by its long EYDF. The spectrum broadens with increasing signal power if we see the spectral evolution at a small wavelength span (Figure 2(d)). The 3 dB bandwidth of the laser spectrum increases to 150 pm at the maximum power of 301 W (Figure 2(e)). The spectral broadening basically monotonically increases with power, which can be explained by nonlinear broadening resulting from four-wave mixing[23]. At high power, the nonlinearity can generate side frequency. Besides, gain shaping is also a broadening factor. To obtain the pump absorption coefficient of the main amplifier, the CLS is removed in the experimental setup to find the total power P_t, including signal and residual pump power. The residual pump power P_p is gained by P_t minus P_s, based on the known signal power P_s. As expected, the residual pump increases as the injected pump power increases (Figure 2(f)). Nonetheless, the pump absorption is only about 6 dB for 50 m long EYDF, and the pump absorption coefficient decreases with increasing pump power (Figure 2(f)). The result partially explains why the optical efficiency is low and the slope efficiency decreases with increasing pump power. Its physical mechanisms should be theoretically studied.

A good splice between EYDF and passive fiber is quite important to keep the beam quality of the laser good and to decrease loss. Due to the existence of a pedestal in EYDF[24] and the large refractive index difference between EYDF and passive fiber, the splice is challenging. In our experiment, spliced heat is optimized to prevent light from entering the pedestal and to minimize loss. The beam quality of the output laser at different powers is measured, as presented in Figure 3(a). Basically, the M^2 value decreases as the output power increases, which indicates the beam quality gets better at higher output power. The phenomenon can be explained by different spatial gains and losses in gain fiber at different pump powers. In the case of no pump power, due to the absorption of the signal laser in fundamental mode by EYDF, the output beam profile of the signal exhibits a donut shape. At this moment, the beam quality is terrible. However, as the pump power increases, gain gradually exceeds absorption and the gain of fundamental mode is dominant in mode competition to make the beam quality slowly improve. At the output power of 301 W, the beam profile at the waist position and hyperbolic fit about the M^2 measurement are presented in Figures 3(b) and 3(c). The M^2 value is measured to be 1.35/1.41 at an output power of 301 W.

The temporal signal of the output laser at different powers is also characterized. At low power, the output laser has a relatively stable time domain (Figure 4(a)). From its probability density function (PDF) of intensity, the PDF is relatively centralized and the peak value of the PDF is nearly at its average intensity $\bar{I}$, which proves its good temporal stability and low extreme event probability (Figure 4(b)). By contrast, at high power, the temporal signal of the laser fluctuates, and more intensity noise is generated (Figure 4(d)). Its PDF is dispersed, and the peak value of the PDF deviates from its average intensity, indicating poor temporal stability (Figure 4(e)). Researchers have reported that PIQ can cause self-pulsing in EDF and EYDF[25–28]. However, the intensity fluctuation we observe here is not like a self-pulse but more like intensity noise, as it is random and has no perfect pulse envelope. Besides, the nonperiodic fluctuation and good

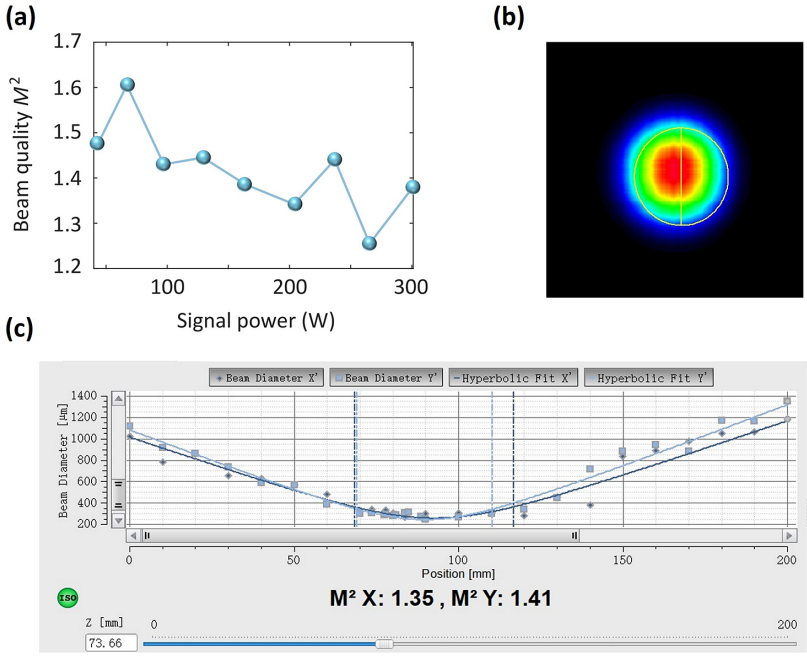

Figure 3. Beam quality of the EYDF amplifier. (a) Beam quality versus output power. At the output power of 301 W, (b) the beam profile at the waist position and (c) the M^2 value are measured.

https://doi.org/10.1017/hpl.2024.20 Published online by Cambridge University Press

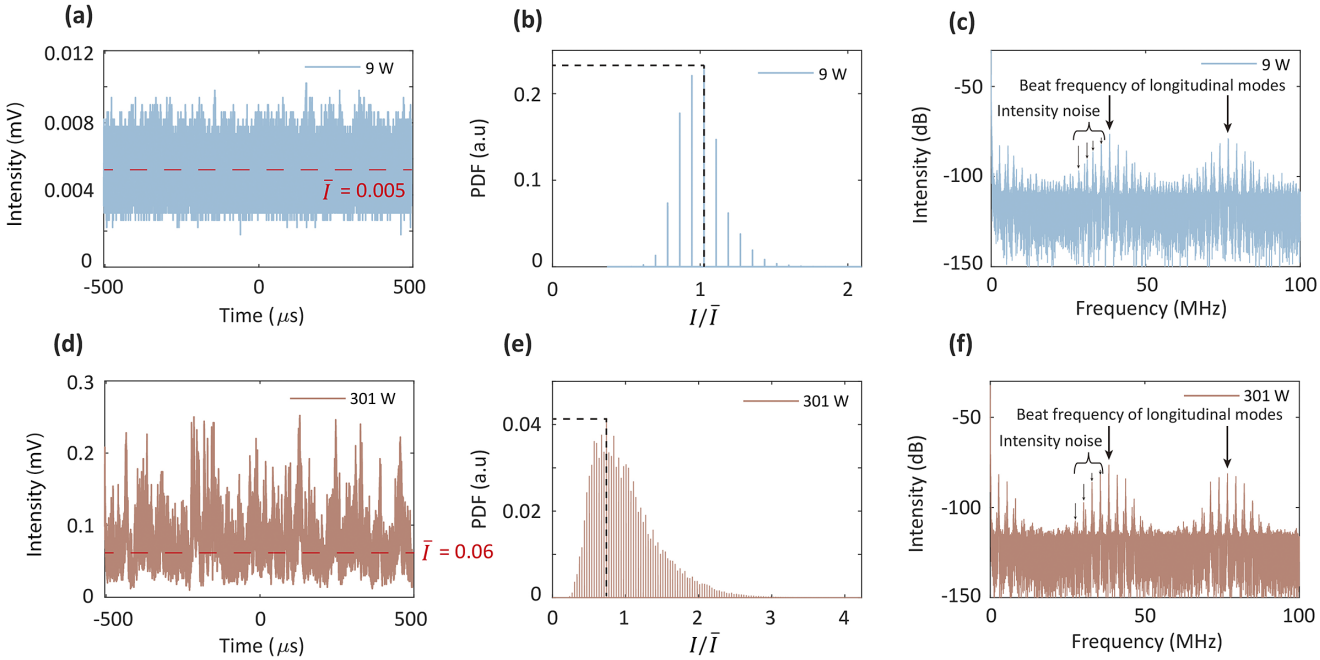

Figure 4. Temporal characteristics of the EYDF amplifier at different output powers. (a)–(c) The temporal signal, its probability density function (PDF) of intensity and its Fourier-transform spectrum at the output power of 9 W, respectively. (d)–(f) The results at the power of 301 W, where $\bar{I}$ is the average intensity of the temporal signal.

beam quality confirm it is not transverse mode instability. In addition, the Fourier-transform spectra are analyzed. The Fourier-transform spectra are both characterized by the beat frequencies of longitudinal modes and noise-induced side frequencies (Figures 4(c) and 4(f)). We infer that the temporal noise may come from the interaction of both PIQ and modulation instability, caused by anomalous dispersion and nonlinearity, which can be further investigated in the future.

4. Model and simulation

4.1. Model of the in-band pumped EYDF amplifier

This section presents mathematical models and simulations to understand the above experimental phenomena. Firstly, we propose a novel dynamic process of ion transition between energy levels for in-band pumped EYDF amplifiers. The simplified erbium energy levels and the ion transitions are illustrated in Figure 5. Level 1 is the ground state $^4I_{15/2}$, levels 2 and 3 are two Stark levels of $^4I_{13/2}$ and level 4 is regarded as $^4I_{9/2}$. After ions on level 1 absorb C band (1535 nm) photons, ions can be excited to pump level 3. Due to the short life of level 3, ions will quickly transmit onto the upper level, namely level 2, by nonradiative transition. Then stimulated emission transition happens from level 2 to level 1. Apart from this, ESA and PIQ are also significant. Because of the in-band pumping, ESA can happen on levels 2 and 3. Pump and signal photons can be absorbed for ion ESA transitions from levels 2 and 3 to level 4. Then, the ions on level 4 will nonradiate to level 2. Actually, ions on level 4

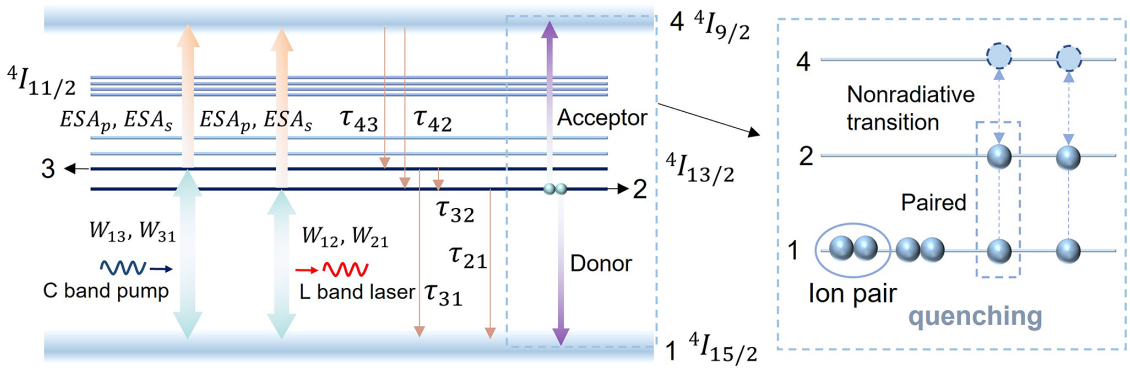

Figure 5. Simplified erbium energy levels and dynamic process of ion transitions for the in-band pumped EYDF amplifier.

https://doi.org/10.1017/hpl.2024.20 Published online by Cambridge University Press

will first jump onto $^4I_{11/2}$, and then transit onto level 2. Therefore, the ESA process will lose energy. It should be noted that ESA at the C band is low, but at the L band it is fairly strong. On the other hand, PIQ also can decrease optical efficiency. When an ion pair is excited to level 2, one ion of the pair will transfer energy to the other[29]. Thus, one ion transits to the ground state, while the other one transits to level 4. The ion on level 4 then will nonradiate to level 2. So, this process wastes pump photons.

Given the above dynamical behavior of ion transitions for the in-band pumped EYDF amplifier, relatively accurate rate equations are proposed, as below:

$$\begin{aligned}\frac{\partial n_{2s}(r,\varphi,z)}{\partial t} &= -\frac{n_{2s}(r,\varphi,z)}{\tau_{21}} + \frac{n_3(r,\varphi,z)}{\tau_{32}} \\ &+ W_{12}(r,\varphi,z)\, n_{1s}(r,\varphi,z) - W_{21}(r,\varphi,z)\, n_{2s}(r,\varphi,z) \\ &- \left(\mathrm{ESA_p}(r,\varphi,z) + \mathrm{ESA_s}(r,\varphi,z)\right) n_{2s}(r,\varphi,z) + \frac{n_4(r,\varphi,z)}{2\tau_{42}},\end{aligned} \tag{1}$$

$$\begin{aligned}\frac{\partial n_3(r,\varphi,z)}{\partial t} &= -\frac{n_3(r,\varphi,z)}{\tau_{32}} - \frac{n_3(r,\varphi,z)}{\tau_{31}} \\ &+ W_{13}(r,\varphi,z)\, n_{1s}(r,\varphi,z) - W_{31}(r,\varphi,z)\, n_3(r,\varphi,z) \\ &- \left(\mathrm{ESA_p}(r,\varphi,z) + \mathrm{ESA_s}(r,\varphi,z)\right) n_3(r,\varphi,z) + \frac{n_4(r,\varphi,z)}{2\tau_{43}},\end{aligned} \tag{2}$$

$$\begin{aligned}\frac{\partial n_4(r,\varphi,z)}{\partial t} &= -\frac{n_4(r,\varphi,z)}{2\tau_{43}} - \frac{n_4(r,\varphi,z)}{2\tau_{42}} \\ &+ \left(\mathrm{ESA_p}(r,\varphi,z) + \mathrm{ESA_s}(r,\varphi,z)\right)\left(n_{2s}(r,\varphi,z) + n_3(r,\varphi,z)\right),\end{aligned} \tag{3}$$

$$\begin{aligned}\frac{\partial n_{2p}(r,\varphi,z)}{\partial t} &= -\frac{n_{2p}(r,\varphi,z)}{\tau_{21}} \\ &+ 2R(r,\varphi,z)\,\frac{n_{1p}(r,\varphi,z) - n_{2p}(r,\varphi,z)}{2} - W(r,\varphi,z)\, n_{2p}(r,\varphi,z),\end{aligned} \tag{4}$$

$$n_{1s}(r,\varphi,z) + n_{2s}(r,\varphi,z) + n_3(r,\varphi,z) + n_4(r,\varphi,z) = 1 - f, \tag{5}$$

$$n_{1p}(r,\varphi,z) + n_{2p}(r,\varphi,z) = f, \tag{6}$$

$$n_2(r,\varphi,z) = n_{2s}(r,\varphi,z) + n_{2p}(r,\varphi,z), \tag{7}$$

$$n_1(r,\varphi,z) = n_{1s}(r,\varphi,z) + n_{1p}(r,\varphi,z), \tag{8}$$

$$W_{12}(r,\varphi,z) = \sum_{i=1}^{m}\left(\frac{\Gamma_{s,i}(r,\varphi)\sum_{j=1}^{N}\left(\sigma_{12,j}\left(P^{+}_{\mathrm{s+ASE},i,j}(z) + P^{-}_{\mathrm{s+ASE},i,j}(z)\right)\lambda_j\right)}{hc}\right), \tag{9}$$

$$W_{21}(r,\varphi,z) = W(r,\varphi,z) = \sum_{i=1}^{m}\left(\frac{\Gamma_{s,i}(r,\varphi)\sum_{j=1}^{N}\left(\sigma_{21,j}\left(P^{+}_{\mathrm{s+ASE},i,j}(z) + P^{-}_{\mathrm{s+ASE},i,j}(z)\right)\lambda_j\right)}{hc}\right), \tag{10}$$

$$W_{13}(r,\varphi,z) = R(r,\varphi,z) = \frac{\Gamma_p(r,\varphi)\,\sigma_{ap}\left(P^{+}_{p}(z) + P^{-}_{p}(z)\right)\lambda_p}{hc}, \tag{11}$$

$$W_{31}(r,\varphi,z) = \frac{\Gamma_p(r,\varphi)\,\sigma_{ep}\left(P^{+}_{p}(z) + P^{-}_{p}(z)\right)\lambda_p}{hc}, \tag{12}$$

$$\mathrm{ESA_p}(r,\varphi,z) = \frac{\Gamma_p(r,\varphi)\,\sigma_{\mathrm{ESA,p}}\left(P^{+}_{p}(z) + P^{-}_{p}(z)\right)\lambda_p}{hc}, \tag{13}$$

$$\mathrm{ESA_s}(r,\varphi,z) = \sum_{i=1}^{m}\left(\frac{\Gamma_{s,i}(r,\varphi)\sum_{j=1}^{N}\left(\sigma_{\mathrm{ESA,s}}\left(P^{+}_{\mathrm{s+ASE},i,j}(z) + P^{-}_{\mathrm{s+ASE},i,j}(z)\right)\lambda_j\right)}{hc}\right), \tag{14}$$

where $n_e(r,\varphi,z)$ is the normalized Er ion population density on the energy level e at the position (r,φ,z) of the fiber, n_{1s}, n_{2s} (n_{1p}, n_{2p}) are single-ion (paired-ion) population density on levels 1 and 2, respectively, and τ_{ek} is relaxation time from level e to level k. In our model, we ignore the intermediate process of ion transition to $^4I_{11/2}$, and consider the direct transition from level 4 to levels 2 and 3. The lifetime of level $^4I_{11/2}$ is much longer than that of level 4, and thus τ_{42} is approximately regarded as the lifetime of level $^4I_{11/2}$ in this model. Besides, since levels 2 and 3 are very close, τ_{42} and τ_{43} are nearly the same. Here, f is the proportion of the ion number of ion pairs in all ions, $\Gamma_p(r,\varphi)$ and $\Gamma_{s,i}(r,\varphi)$ are power filling distributions for the pump and signal in mode i, respectively, m and N are the number of spatial modes and spectral bins, respectively, σ_{ap} and σ_{ep} are the absorption and emission cross-sections at the pump wavelength, $\sigma_{12,j}$ and $\sigma_{21,j}$ are the absorption and emission cross-sections at the signal wavelength of λ_j and $\sigma_{\mathrm{ESA,p}}$ ($\sigma_{\mathrm{ESA,s}}$) is the absorption cross-section for ESA at the pump wavelength (signal wavelength). Because most of the power is occupied by the central wavelength (1585 nm), in our simulation we hypothesize that all signal wavelengths λ_j have the same $\sigma_{\mathrm{ESA,s}}$ as the center wavelength. Further h, c are the Planck constant and light speed, respectively, W_{ek} denotes transfer rate from level e to k for single ions, W and R denote the transfer rate for ion pairs, $\mathrm{ESA_p}$ ($\mathrm{ESA_s}$) is the transfer rate of ESA at the pump (signal) wavelength, $P^{\pm}_{p}(z)$ is the power of the forward (+) and reverse (−) pump laser at the z position and $P^{\pm}_{\mathrm{s+ASE},i,j}(z)$ is the power of the forward and reverse signal laser, including ASE in mode i at the wavelength of λ_j at the z position. Because of forward pumping, only the forward pump and signal laser are considered in our simulation.

The power propagation equations in EYDF are written as follows:

$$\begin{aligned}\pm\frac{\mathrm{d}P^{\pm}_{p}(z)}{\mathrm{d}z} = \Bigg(&\int_0^{2\pi}\int_0^{a}\Big(n_3(r,\varphi,z)\,\sigma_{ep}N_{er} \\ &- n_1(r,\varphi,z)\,\sigma_{ap}N_{er}\Big)\Gamma_p(r,\varphi)\,r\mathrm{d}r\mathrm{d}\varphi - \alpha_p\Bigg)P^{\pm}_{p}(z),\end{aligned} \tag{15}$$

https://doi.org/10.1017/hpl.2024.20 Published online by Cambridge University Press

$$\pm\frac{dP^{\pm}_{s+ASE,i,j}(z)}{dz}=\left(\sigma_{21,j}N_{er}\int_0^{2\pi}\int_0^{a}n_2(r,\varphi,z)\,\Gamma_{s,i}(r,\varphi)\,r\,dr\,d\varphi\right.$$
$$\left.-\sigma_{12,j}N_{er}\int_0^{2\pi}\int_0^{a}n_1(r,\varphi,z)\,\Gamma_{s,i}(r,\varphi)\,r\,dr\,d\varphi-\alpha_s-l_{b,i}\right)P^{\pm}_{s+ASE,i,j}(z)$$
$$+\frac{4hc^2}{\lambda_j^3}\sigma_{21,j}N_{er}\Delta\lambda\int_0^{2\pi}\int_0^{a}n_2(r,\varphi,z)\,\Gamma_{s,i}(r,\varphi)\,r\,dr\,d\varphi, \quad (16)$$

where a is the radius of the fiber core, N_{er} is the total doping concentration of EYDF, α_p, α_s are the intrinsic loss of EYDF at the pump wavelength and signal wavelength, respectively, $l_{b,i}$ is the bending loss of mode i and $\Delta\lambda$ is the width of adjacent spectral bins.

Due to the high output power and noise pulse in EYDF, the multimode nonlinear Schrodinger equation is applied[30–32]. The equation considers dispersion and nonlinear effects for simulating spectral nonlinear broadening and intermodal coupling.

The above equations form a spatial-mode-resolved nonlinearity-assisted model, including rate equations, propagation equations and a multimode nonlinear Schrodinger equation, capable of simulating the power distribution, laser spectrum and beam profile. This kind of modeling method has been used in other nonlinear multimode gain systems, such as ultrafast multimode gain fiber, and the basic idea and calculated methods are explained in detail in Refs. [33–35]. The related parameters used in the simulation are listed in Table 1.

4.2. Simulation of the in-band pumped EYDF amplifier

Simulations of the main amplifier are conducted in this section using the model above. The output laser of the second pre-amplifier is regarded as the seed laser of the main amplifier. The fabricated seed has the same features as the seed used in the experiment, with a power of 30 W, a central wavelength of 1585 nm, a bandwidth of 57.5 pm and a signal-to-noise ratio of 40 dB. The shot noise of the seed is also considered by adding a certain number of photons with a random phase to each spectral bin[36]. The initial excitation condition (amplitude ratio among spatial modes) is set as (1, 0.4, 0.4, 0.2, 0.2), so the fundamental mode has the highest injected power. To match the experimental results, f is reasonably set.

After the simulation parameters are appropriately set, the simulation results are as depicted in Figure 6. As can be seen, the simulated output power (Figure 6(a)) and slope efficiency (Figure 6(b)) are in good agreement with the experimental results, except for the pump absorption (Figure 6(c)). The simulation results confirm the experimental findings that optical efficiency is low and that pump absorption and slope efficiency drop with increasing pump power. The measured pump absorption is actually smaller than the true value. Since it is measured by removing and installing the CLS after the main amplifier, the signal in the fiber's pedestal can also be stripped[24], which makes pump absorption a little low. In general, the simulation results are relatively accurate. When the pump power is 2300 W, the power distribution of each spatial mode in the fiber (Figure 6(d)), output spectrum (Figure 6(e)) and spectral evolution in the fiber (Figure 6(f)) are simulated. It can be seen that in the EYDF each spatial mode is amplified, while the fundamental mode dominates to improve beam quality. The output spectrum is a combined spectrum of all spatial modes, featuring weak short-wavelength and long-wavelength ASE (Figure 6(e)), which qualitatively agrees with the experimental results. The ASE is the result of the interaction between the signal spectrum and gain spectrum. At the beginning of amplification, the gain peak is centered at the short wavelength, so the short-wavelength ASE on the spectrum comes out (Figure 6(f)). As the transmission continues, due to the gain redshift, the short-wavelength ASE recedes and the long-wavelength ASE is amplified (Figure 6(f)).

To see the gain redshifts clearly, the centroid evolution of the gain spectrum in the EYDF is displayed in Figure 7(a). Note that when light travels through the whole EYDF, the center of the gain spectrum gradually redshifts, which causes different spectral components of the signal light to have

Table 1. Some parameters used in the simulation.

Sym./unit	Physical meaning	Value
N_{er}/m^{-3}	Er ion concentration	2.3×10^{25}
f	The proportion of the number of paired ions	0.16
σ_{ap}/m^2	Absorption cross–section at the pump wavelength	4.74×10^{-25}
σ_{ep}/m^2	Emission cross–section at the pump wavelength	4.75×10^{-25}
$\sigma_{12,j}\left(\sigma_{21,j}\right)/m^2$	Absorption (emission) cross–section at signal wavelength λ_j	Ref. [20]
$\sigma_{ESA,p}/m^2$	Absorption cross–section for ESA at 1535 nm	8.06×10^{-26}
$\sigma_{ESA,s}/m^2$	Absorption cross–section for ESA at 1585 nm	3.07×10^{-25}
τ_{21}/s	Relaxation time for level 2 ($^4I_{13/2}$) → level 1 ($^4I_{15/2}$)	7×10^{-3}
τ_{31}/s	Relaxation time for level 3 ($^4I_{13/2}$) → level 1($^4I_{15/2}$)	7×10^{-3}
τ_{32}/s	Relaxation time for level 3 ($^4I_{13/2}$) → level 2 ($^4I_{13/2}$)	1×10^{-12}
τ_{43}/s	Relaxation time for level 4 ($^4I_{9/2}$) → level 3 ($^4I_{13/2}$)	5.2×10^{-6}
τ_{42}/s	Relaxation time for level 4 ($^4I_{9/2}$) → level 2 ($^4I_{13/2}$)	5.2×10^{-6}

https://doi.org/10.1017/hpl.2024.20 Published online by Cambridge University Press

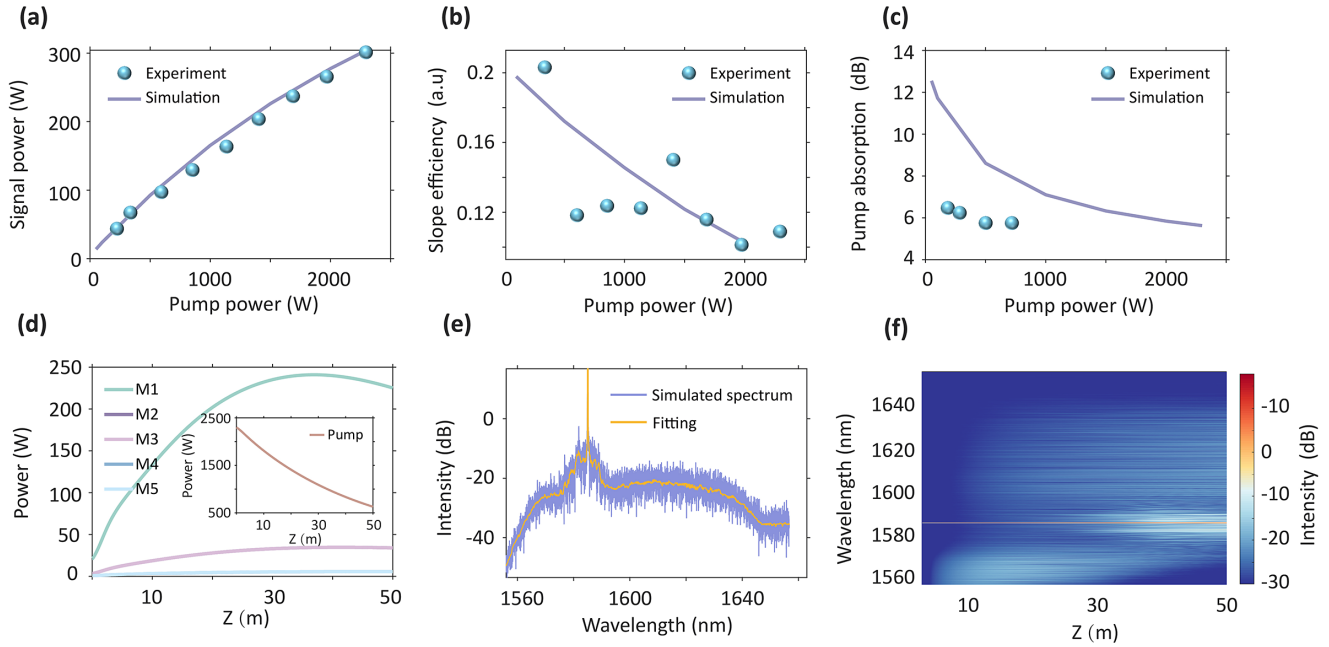

Figure 6. Simulation results of the in-band pumped EYDF amplifier. (a) Output signal power, (b) slope efficiency and (c) pump absorption versus pump power in the simulation and experiment. At the pump power of 2300 W, (d) power distribution of each spatial mode along the EYDF, (e) output spectrum and (f) spectral evolution in the fiber. M1, M2, M3, M4, M5 represent LP01, LP11a, LP11b, LP21a, LP21b modes, respectively.

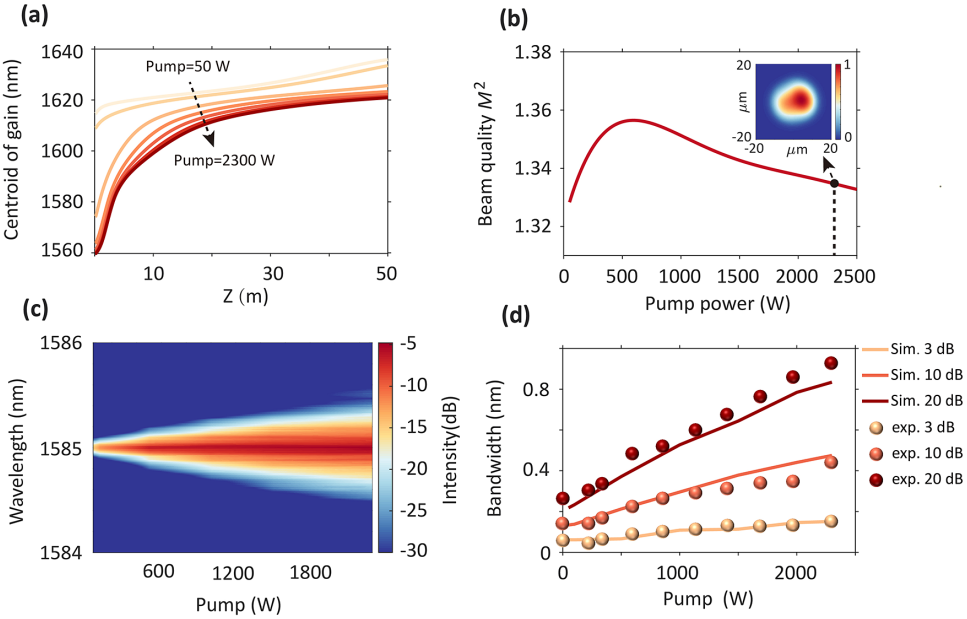

Figure 7. Characteristics of the output laser for different pump powers in simulation. (a) Variation of the centroid of the gain spectrum (gain redshift) in the gain fiber with pump power. (b) Beam quality of the output laser versus pump power. The inset exhibits the beam profile of the output laser at the pump power of 2300 W. (c) Spectral evolution at different pump powers. (d) The output laser's 3, 10 and 20 dB bandwidths under different pump powers in our simulation and experiment.

different gains at different positions of the fiber. Besides, as the pump power increases, the gain-saturated velocity of short-wavelength components becomes slow, so the gain spectrum blueshifts with the pump power. So, as the pump power increases, the long-wavelength ASE on the output spectrum will be suppressed. In the spatial domain, the beam quality varying with pump power is also simulated, as presented in Figure 7(b). It manifests that the beam quality of the signal laser degrades first, and then becomes better as the pump power increases. The inset in Figure 7(b) exhibits the simulated beam profile of the output laser at the pump power of 2300 W. The simulated result of beam self-cleaning agrees with the experimental phenomenon. It indicates that the signal laser experiences different spatial

https://doi.org/10.1017/hpl.2024.20 Published online by Cambridge University Press

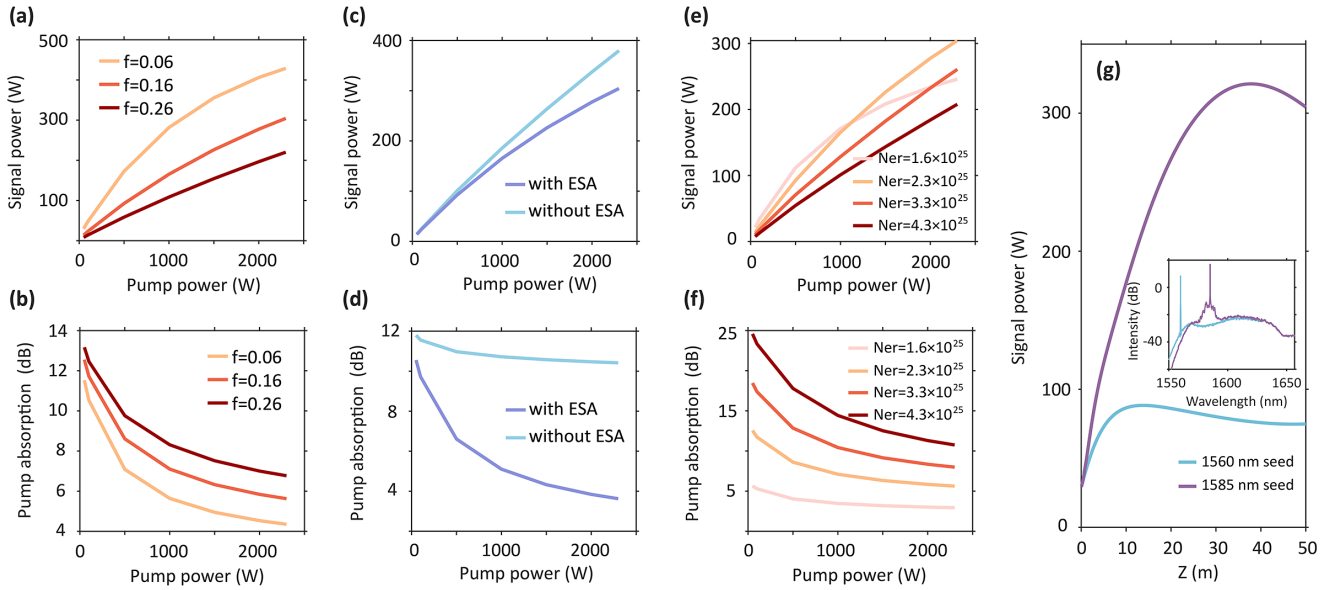

Figure 8. Effect of PIQ, ESA, Er ion concentration and seed wavelength on the EYDF amplifier. (a) Effect of PIQ on output signal power and (b) pump absorption of the EYDF. (c) Effect of ESA on output signal power and (d) pump absorption. (e), (f) Results about the impact of Er ion concentrations. (g) Impact of the seed wavelength on signal power and output spectrum. The inset shows output spectra for different-wavelength seeds.

gains and losses at different pump powers, as explained in the experimental part. Note that at low pump power, the beam quality degrades, because the gain provided by the pump cannot compensate for the absorption of EYDF. However, as the pump power is high enough, the gain exceeds the loss and the gain of the fundamental mode is dominant, so the beam becomes clean. Applying the theoretical model, the spectral broadening with pump power can also be simulated, as shown in Figure 7(c). Because of the increased nonlinearity, as the pump power increases from 50 to 2300 W, the 3, 10 and 20 dB spectral bandwidths of the laser widen from 0.06 to 0.15 nm, from 0.13 to 0.47 nm and from 0.22 to 0.83 nm, respectively (Figure 7(d)). The simulated broadening bandwidth matches the experimental results, qualitatively and quantitatively.

It is known that the in-band pumping has a low quantum defect, which contributes to improving laser efficiency. However, the output power in our experiment and simulation is not as expected, which triggers us to wonder about the internal mechanisms and to search for optimized methods to improve the output power. Here, we study the impacts of PIQ, ESA, Er ion concentration and seed wavelength on the laser system, as presented in Figure 8. When investigating one specific parameter, other parameters are kept unchanged. PIQ is an essential factor inhibiting power enhancement. As PIQ becomes severe, namely as f grows, the output power decreases quickly, whereas the pump absorption increases (Figures 8(a) and 8(b)). This is because the severe PIQ brings a more extensive heat dissipation, which decreases system efficiency. The impact mechanism of PIQ on pump absorption will be discussed later in Figure 9. ESA also plays an important role. Two scenarios are compared. One simulation includes ESA, whereas the other one excludes ESA. As seen in Figures 8(c) and 8(d), ESA can considerably reduce the output power, slope efficiency and pump absorption. The findings verify that ESA is the major factor in decreasing slope efficiency and pump absorption with increasing pump power. As shown in Figure 8(c), the effect of PIQ on laser power is linear with pump power, but the impact of ESA is nonlinear. The reason is associated with the ion distributions among energy levels, which will be discussed later. Furthermore, Er ion concentration is changed to see its impact on the system. Generally, the PIQ effect will be enhanced with the increase of doping concentration, but the PIQ can remain unchanged if the ratio of Yb and other components is optimized. One can see from Figures 8(e) and 8(f) that as the concentration increases, the output power first grows and then gets lower at high pump powers, and the pump absorption rises. When PIQ is significant, too high a concentration will not boost output power, but will reduce optical efficiency. The increasing pump absorption is due to more pump photons absorbed by more ions. Finally, it is demonstrated that choosing an appropriate seed wavelength is significant. Simulation results obtained with different seed wavelengths are depicted in Figure 8(g), where signal power evolutions along the fiber and output spectra for 1560 and 1585 nm seeds are compared. Notably, the case using the 1560 nm seed has very low efficiency and the output spectrum has strong long-wavelength ASE. This case is dangerous, because ASE-induced giant pulses can damage the fiber system. In contrast, when using the 1585 nm seed, the efficiency is higher and ASE is restrained because the signal achieves maximum gain by matching the signal wavelength and gain distribution in the long EYDF.

https://doi.org/10.1017/hpl.2024.20 Published online by Cambridge University Press

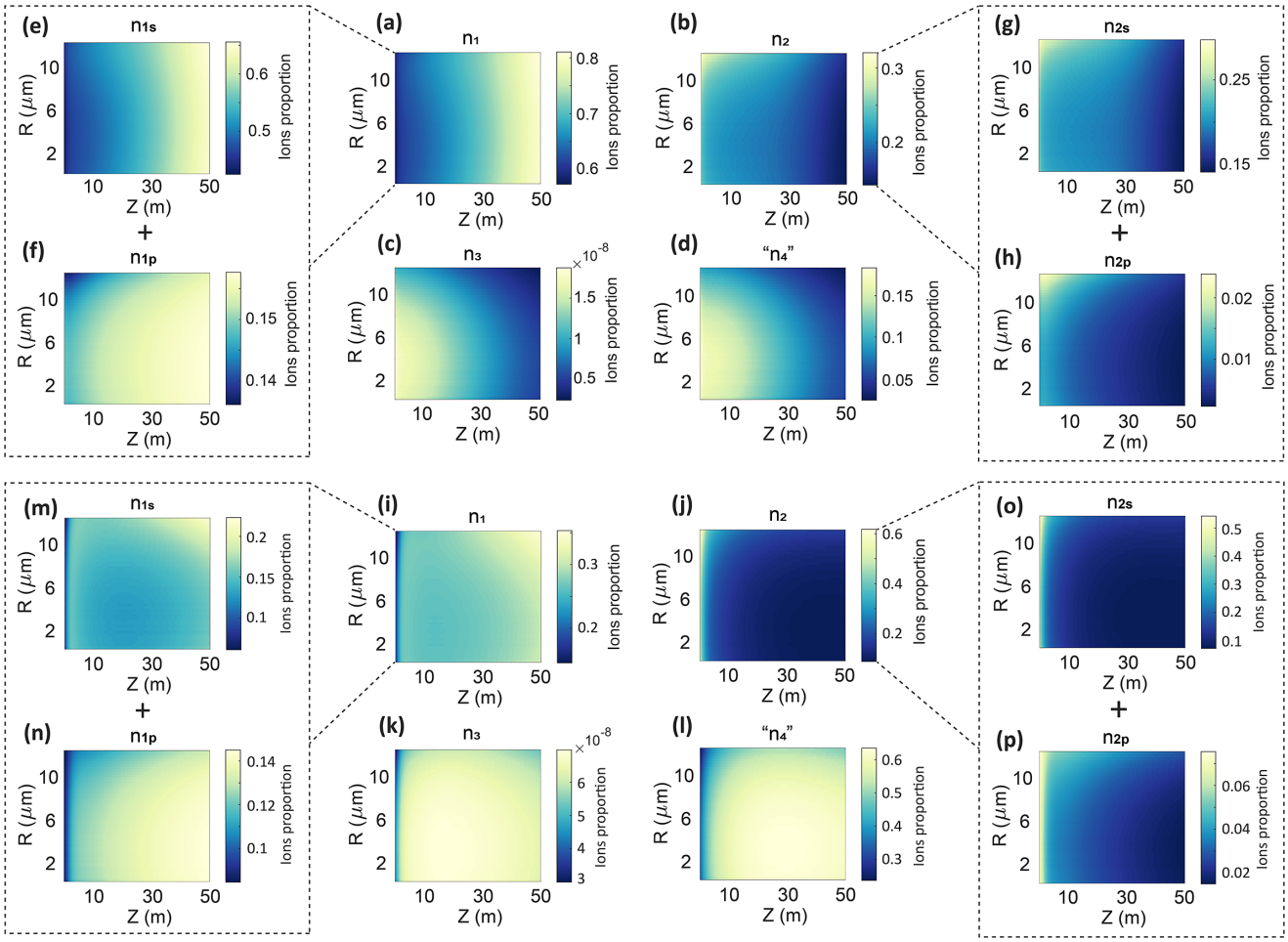

Figure 9. Distributions of erbium ions among energy levels on the cross-section (R) and along the Z-axis of the fiber at different pump powers. (a)–(d), (i)–(l) The ion distributions of levels 1–'4' at the pump powers of 50 and 2300 W, respectively. (e), (f) Single-ion and paired-ion distributions on level 1 at the pump power of 50 W, respectively. (g), (h) Single-ion and paired-ion distributions on level 2 at the pump power of 50 W, respectively. (m), (n) Single-ion and paired-ion distributions on level 1 at the pump power of 2300 W, respectively. (o), (p) Single-ion and paired-ion distributions on level 2 at the pump power of 2300 W, respectively. The ion number on level '4' is the sum of ions on level 4 and level $^4I_{11/2}$.

Here, we explore the dynamic impact mechanisms of ESA and PIQ on laser efficiency, pump absorption and gain distribution to understand the experiment and simulation results better. The ion distributions among energy levels at different pump powers are simulated. Figures 9(a)–9(h) exhibit the normalized concentration distributions of ions on the cross-section and along the Z-axis of the fiber at the pump power of 50 W. Figures 9(i)–9(p) show the results at the pump power of 2300 W. The sum of ion concentration of all energy levels (n_1–'n_4') is a 2D matrix where each element is 1 to prove the normalized ion concentration. By comparing the ion distributions for different pump powers, the following conclusions are obtained. (1) As the pump power increases, more ions are excited from level 1 to the upper level (level 2) at the injected end of the EYDF to produce higher gain (Figures 9(a), 9(b), 9(i) and 9(j)), but surprisingly most of the ions in the entire EYDF are not on level 2 but on level '4', except at the injected end of the EYDF. At high pump power, level 2 has only about 20% of ions at most locations within the fiber (Figure 9(j)), which is not conducive to enable high laser efficiency. (2) In addition, the ion pairs almost do not change much on levels 1 and 2 with the change of pump power, but single ions are mainly involved in the variation (Figures 9(e)–9(h) and 9(m)–9(p)), which may explain why the impact of PIQ on output power is linear with pump power. (3) Almost all ion pairs are on level 1 at different pump powers. This indicates that if the fiber has a strong PIQ, the ion number on level 1 will grow, which indeed helps improve the pump absorption of the EYDF. (4) Notably, level 3 is nearly empty because of its short lifetime (Figures 9(c) and 9(k)). As the pump power increases, the ion number on level '4' grows considerably due to ESA (Figures 9(d) and 9(l)). As mentioned before, level 4 has a very short lifetime and τ_{42} is approximately regarded as the lifetime of level $^4I_{11/2}$. Hence, true level 4 has almost no ions. Here the ion number on level '4' is seen as the sum of ions on level 4 and level $^4I_{11/2}$. As seen from Figure 9(l), for most of the locations within the EYDF, nearly 60% of ions transit

https://doi.org/10.1017/hpl.2024.20 Published online by Cambridge University Press

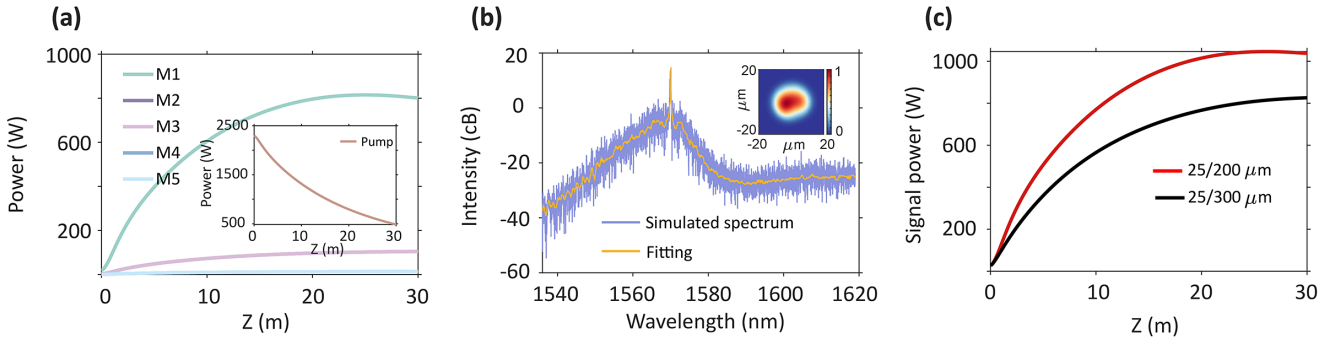

Figure 10. Simulated results of the optimized in-band pumped EYDF amplifier. (a) Signal power distribution across all spatial modes in the EYDF. The inset shows the pump power distribution in the EYDF. (b) Output signal spectrum at the pump power of 2300 W. The inset exhibits the beam profile of the output laser. (c) Signal power distributions along the fiber for two EYDFs with different core-to-cladding ratios at the pump power of 2300 W.

onto level '4', which severely reduces the laser efficiency. In terms of pump absorption, at higher pump power more ions will be on level '4', so the ions involving pump absorption on level 1 will be less; in turn, the pump absorption will decrease with increasing pump power. Because of that, the reason why the effect of ESA on signal power and pump absorption is nonlinear with pump power is revealed.

To improve the laser efficiency of the in-band pumped EYDF amplifier, various approaches are proposed here to optimize the fiber system. Firstly, increase the Er ion concentration of EYDF while inhibiting PIQ. A higher concentration means that PIQ is more likely to occur. To suppress PIQ, Yb ion concentration and other components in EYDF should be optimized simultaneously[16,24,37], which is a high requirement for the manufacture of EYDF. Secondly, considering the ability to withstand high pump power, the core-to-cladding ratio of EYDF should be larger. Increasing the core-to-cladding ratio can significantly improve pump absorption coefficient and laser efficiency. Thirdly, select the appropriate length of EYDF and avoid obsessing over pursuing the pump absorption coefficient. Because of ESA, the pump absorption is much lower than the value given by manufacturers. Hence, much longer EYDF may be used. While it is true that longer EYDF absorbs more pump power, it may bring a negative consequence – self-absorption. Self-absorption can cause signal absorption by EYDF, thereby reducing the laser efficiency. Last but not least, choose an appropriate central wavelength of seed. The selection of the central wavelength needs to consider two aspects. On the one hand, the fiber length needs to be considered. The fiber length affects the range of gain redshift. According to our experience, in main amplifiers, long EYDF usually will be used, so a central wavelength of a seed of more than or equal to 1570 nm is a reasonable choice. On the other hand, the influence of ESA should be considered. It is good to choose the central wavelength of less than or equal to 1585 nm, because the ESA will be severe to inhibit efficiency as increasing the central wavelength.

Utilizing the optimized methods mentioned above, we simulate an optimized EYDF amplifier with the following parameters: $f$of 0.01, seed wavelength of 1570 nm, Er ion concentration of 4.34×10^{25} m^{-3}, fiber size of 25/200 μm, core NA of 0.09, fiber length of 30 m and initial excitation condition of (1, 0.4, 0.4, 0.2, 0.2). The simulation results are plotted in Figure 10. The signal power distribution across all spatial modes in the EYDF indicates a substantial improvement, with the total output power reaching nearly 1 kW (Figure 10(a)). The optical efficiency is enhanced by 30.5% compared with experimental results. The inset in Figure 10(a) shows the pump power distribution in the fiber. The spectrum of the output laser is illustrated in Figure 10(b), which manifests intense broadening of the spectral pedestal due to higher nonlinearity. The inset in Figure 10(b) exhibits the output laser's beam profile with M^2 of 1.29. Figure 10(c) shows the power comparison of two EYDFs with different core-to-cladding ratios at the pump power of 2300 W. It suggests that the output power of EYDF with a high core-to-cladding ratio (25/200 μm) is 25% higher than that with a low core-to-cladding ratio (25/300 μm).

5. Conclusion

In summary, we numerically and experimentally verify the underlying capability of in-band pumped EYDF amplifiers in enabling higher output power. A 301 W narrow-linewidth EYDF amplifier operating at 1585 nm with good beam quality has been experimentally and numerically demonstrated using kilowatt-level 1535 nm fiber laser in-band pumping. As far as we know, it is the highest output power achieved in L-band narrow-linewidth fiber amplifiers with a good beam quality of $M^2 <$ 1.4. The power is limited by heat damage of the fusion-splicing point. The 3 dB bandwidth is about 150 pm at the highest power. The temporal stability of the output laser is found to become worse with increasing power. The temporal noise may come from the interaction

https://doi.org/10.1017/hpl.2024.20 Published online by Cambridge University Press

of both PIQ and modulation instability. Meanwhile, given our proposed ion transition behavior for in-band pumping, a spatial-mode-resolved nonlinearity-assisted theoretical model is established to depict the physical mechanisms in EYDF amplifiers for the first time. The model can relatively accurately simulate experimental results, for example, output power, spectral broadening and beam quality. Simulation verifies that PIQ and ESA are the significant factors for the decrease in optical efficiency. The difference is that the effect of PIQ on output power is linear, but the ESA effect is nonlinear. ESA can decrease pump absorption and slope efficiency with increasing pump power. Furthermore, the distributions of erbium ions among energy levels are obtained by our simulation to help us understand the dynamic process for in-band pumped EYDF amplifiers. Results show that all ion pairs are almost on the ground level, and their number hardly changes with increasing pump power to indicate the linear influence of PIQ. Nonetheless, as the pump power increases, the ion number on level '4' dramatically grows, which gradually inhibits the laser efficiency to explain the nonlinear effect of ESA. Finally, some optimized approaches are proposed to demonstrate a 1-kW in-band pumped EYDF amplifier, such as suppressing ESA and PIQ, increasing the doping concentration, optimizing the fiber length, increasing the core-to-cladding ratio and optimizing the central wavelength. We believe that in-band pumped EYDF amplifiers have great potential to enable near diffraction-limited higher power output at the L band in the future if EYDF is appropriately optimized.

Acknowledgement

This work was supported by the National Natural Science Foundation of China (Nos. 62122040, 62075113 and 61875103).

References

1. J. W. Nicholson, A. Grimes, A. Hariharan, V. Sudarshanam, C. Jin, and I. Sun, in *Optical Fiber Communication Conference* (2023), paper Th3C.7.
2. D. Y. Song, J. W. Cho, Y. S. Hurh, J. H. Lim, D. W. Lee, J. S. Lee, K. W. Lee, and K. J. Chang, Opt. Express **7**, 280 (2000).
3. O. De Varona, W. Fittkau, P. Booker, T. Theeg, M. Steinke, D. Kracht, J. Neumann, and P. Wessels, Opt. Express **25**, 24880 (2017).
4. N. Mavalvala, D. E. McClelland, G. Mueller, D. H. Reitze, R. Schnabel, and B. Willke, Gen. Relativ. Gravit. **43**, 569 (2011).
5. C. Wang, H. Xia, M. Shangguan, Y. Wu, L. Wang, L. Zhao, J. Qiu, and R. Zhang, Opt. Express **25**, 20663 (2017).
6. M. Meleshkevich, N. Platonov, D. Gapontsev, A. Drozhzhin, V. Sergeev, and V. Gapontsev, in *2007 European Conference on Lasers and Electro-Optics and the International Quantum Electronics Conference* (2017), p. 1.
7. J. D. Minelly, W. L. Barnes, R. I. Laming, P. R. Morkel, J. E. Townsend, S. G. Grubb, and D. N. Payne, IEEE Photonics Technol. Lett. **5**, 301 (1993).
8. B. Shiner, in *CLEO* (2013), paper AF2J.1.
9. B. M. Anderson, J. Solomon, and A. Flores, Proc. SPIE **11665**, 116650B (2021).
10. Y. Jeong, S. Yoo, C. A. Codemard, J. Nilsson, J. K. Sahu, D. N. Payne, R. Horley, P. W. Turner, L. Hickey, A. Harker, M. Lovelady, and A. Piper, IEEE J. Sel. Tocp. Quantum Electron. **13**, 573 (2007).
11. T. Matniyaz, F. Kong, M. T. Kalichevsky-Dong, and L. Dong, Opt. Lett. **45**, 2910 (2020).
12. J. Huang, Q. Zhao, J. Zheng, C. Huang, Q. Gu, W. Jiang, K. Zhou, C. Yang, Z. Feng, Q. Zhang, Z. Yang, and S. Xu, Photonics **9**, 396 (2022).
13. W. Li, Q. Qiu, L. Yu, Z. Gu, L. He, S. Liu, X. Yin, X. Zhao, J. Peng, H. Li, Y. Xing, Y. Chu, N. Dai, and J. Li, Opt. Lett. **48**, 3027 (2023).
14. W. Yu, Q. Xiao, L. Wang, Y. Zhao, T. Qi, P. Yan, and M. Gong, Opt. Lett. **46**, 2192 (2021).
15. J. Zhang, V. Fromzel, and M. Dubinskii, Opt. Express **19**, 5574 (2011).
16. M. A. Jebali, J.-N. Maran, and S. LaRochelle, Opt. Lett. **39**, 3974 (2014).
17. X. Cheng, Z. Lin, X. Yang, S. Cui, X. Zeng, H. Jiang, and Y. Feng, High Power Laser Sci. Eng. **10**, e3 (2022).
18. X. Guan, Q. Zhao, W. Lin, T. Tan, C. Yang, P. Ma, Z. Yang, and S. Xu, Photonics Res. **8**, 414 (2020).
19. W. Dan, Q. Han, Q. Jia, K. Ren, and T. Liu, Appl. Opt. **60**, 2560 (2021).
20. W. Yu, P. Yan, Q. Xiao, T. Qi, D. Li, and M. Gong, Appl. Opt. **60**, 2046 (2021).
21. L. Dong, T. Matniyaz, M. T. Kalichevsky-Dong, J. Nilsson, and Y. Jeong, Opt. Express **28**, 16244 (2020).
22. W. Yu, P. Yan, T. Qi, Y. Wu, D. Li, Q. Xiao, and M. Gong, Opt. Express **30**, 16837 (2022).
23. S. Du, G. Fu, T. Qi, C. Li, Z. Huang, D. Li, P. Yan, M. Gong, and Q. Xiao, Opt. Fiber Technol. **73**, 103011 (2022).
24. M. M. Khudyakov, A. S. Lobanov, D. S. Lipatov, K. K. Bobkov, S. S. Aleshkina, T. A. Kochergina, M. M. Bubnov, A. N. Abramov, N. N. Vechkanov, A. N. Guryanov, and M. E. Likhachev, Proc. SPIE **10914**, 109141R (2019).
25. F. Sanchez, P. L. Boudec, P. L. Frangois, and G. Stephan, Phys. Rev. A **48**, 2220 (1993).
26. H. Lin, Y. Feng, P. Barua, J. K. Sahu, and J. Nilsson, in *Laser Congress 2017* (2017), paper ATh4A.2.
27. L. Agrawal and D. Ganotra, Appl. Phys. B Lasers Opt. **126**, 14 (2020).
28. J. Shang, T. Feng, S. Zhao, J. Zhao, Y. Zhao, Y. Song, and T. Li, Appl. Phys. Express **13**, 112006 (2020).
29. J. Nilsson, B. Jaskorzynska, and P. Blixt, IEEE Photonics Technol. Lett. **5**, 1427 (1993).
30. G. Fu, J. Tian, T. Qi, Y. Wu, Y. Zhao, Q. Xiao, D. Li, M. Gong, and P. Yan, Opt. Express **30**, 39086 (2022).
31. G. Fu, T. Qi, W. Yu, L. Wang, Y. Wu, X. Pan, Q. Xiao, D. Li, M. Gong, and P. Yan, Laser Photonics Rev. **17**, 2200987 (2023).
32. P. Horak and F. Poletti, in *Recent Progress in Optical Fiber Research* (IntechOpen, 2012), p. 3.
33. G. Fu, D. Li, M. Gong, P. Yan, and Q. Xiao, Appl. Phys. Lett. **123**, 091106 (2023).
34. Y.-H. Chen, H. Haig, Y. Wu, Z. Ziegler, and F. Wise, J. Opt. Soc. Am. B **40**, 2633 (2023).
35. L. Yin, Z. Han, and R. Shu, Opt. Express **31**, 10840 (2023).
36. J. M. Dudley, G. Genty, and S. Coen, Rev. Mod. Phys. **78**, 1135 (2006).
37. M. M. Khudyakov, A. S. Lobanov, D. S. Lipatov, A. N. Abramov, N. N. Vechkanov, A. N. Guryanov, M. A. Melkumov, K. K. Bobkov, S. S. Aleshkina, T. A. Kochergina, L. D. Iskhakova, F. O. Milovich, M. M. Bubnov, and M. E. Likhachev, Laser Phys. Lett. **16**, 025105 (2019).

https://doi.org/10.1017/hpl.2024.20 Published online by Cambridge University Press